

Innovative Electric Propulsion trends, concurrent mission design and enabling technologies for a bold CubeSat Lunar Positioning System

M.Wijnen, S.Correyero-Plaza, N.Agüera-López, D.Peréz-Grande

June 2017

Abstract

CubeSats have become exceedingly versatile satellite platforms over the last decade. However they are still limited by a lack of efficient propulsive means. A novel electric thruster based on Electron Cyclotron Resonance heating and Magnetic Nozzle acceleration may provide a suitable yet simple solution. This device, while currently providing 1000s I_{sp} and 1 mN of thrust at 30W of power, may enable Lunar CubeSat missions from GEO using on-board propulsion. An example mission to provide GPS on the lunar surface using 3U CubeSats in a 60°:24/4/1 Walker constellation with a semi-major axis of 4000 km is proposed; a preliminary assessment of this mission, together with the satellite architecture and cost, is performed. Concurrent trajectory design for very-low-energy transfers is used to demonstrate the feasibility of the mission and its influence on the space-craft design.

1 Introduction

One of the biggest trends in space technology is miniaturization. Currently 762 nanosatellites have been launched [1], accounting for nearly 10% of all spacecraft ever launched. Part of their success has been due the CubeSat standard which 699 out of those 762 nanosatellites abide by. Technology in the field of miniaturization is rapidly advancing increasing the capabilities of CubeSats. The main constraint on CubeSats however has been the restricted propulsive capabilities, which limit the breadth of missions that these satellites may carry out. Presently, a number of bold missions are being proposed for these satellite platforms: Lunar IceCube [2] and AstroCube are examples of Lunar and Deep Space exploration, respectively, unlocked through the use of on-board miniaturized electric propulsion systems.

CubeSat propulsive technologies have been “historically” limited to hot and cold gas thrusters and resisto-jets, which provide relatively high thrust but low I_{sp} ; high energy density mono or bi-propellant systems are heavily restricted in “piggy-backing” CubeSats, as to not pose a threat to the main mission payload. Therefore, more competitive technologies have arised, including miniature ion thrusters and electrospray thrusters; however, these technologies can be complex and expensive. The ion thruster requires fairly high power and generally requires a neutralizer, while the electrospray thrusters are limited by specialized propellants and present manufacturing challenges. On the contrary, the Electron Cyclotron Resonance (ECR) Magnetic Nozzle thruster, a.k.a. ECR Accelerator (ECRA), appears to be a simple (and potentially cheap) device capable of providing competitive propulsive capabilities at low power. The use of ECRA thruster could thus greatly enhance the operational range of CubeSats allowing for deep space and Lunar CubeSat missions at costs acceptable within the CubeSat standard.

Recently several space agencies have shown renewed interest in Lunar exploration with both manned and unmanned missions. A Lunar GPS, or Lunar Positioning System (LPS), would enable future missions to the moon providing on-surface navigational aid. A Walker constellation of 24 CubeSats with a 4000 km semi-major axis would provide full coverage even at the poles. The current manuscript considers using the ECRA for this mission because it has the simplest design of current developing technologies (no neutralizer,

no grids, no fragile parts) while already showing promising performances. It would allow the CubeSats to reach Lunar orbit from GEO, perform orbit insertion, plane change and station-keeping for several years.

The applications of an LPS are many, ranging from unmanned exploration missions to potential future manned missions and colonies on the moon, which are within plan for most of the major space agencies. A very early application for this technology, which also helps to further advance the paradigm change that CubeSats are bringing, would be JAXA's OMOTENASHI 6U Lunar lander which is planned to piggy-back on the Exploration-Mission-1, in the maiden launch of NASA's Space Launch System. The trajectory determination for the final Moon approach and landing was observed to be crucial to that mission by Hernando-Ayuso [3], and the current proposal requires the use of NASA's Deep Space Network, which is costly; a readily available LPS, such as the one described in this paper, would provide the reliability and positioning capabilities required by such a landing mission at a fraction of the cost.

The paper is structured as follows: first, the current version of ECRA is introduced, including subsystem design, some novel enabling technologies and reasonable performance trends. Then, the low thrust trajectory optimization assuming the propulsive capabilities of the ECRA will be presented: the optimization is used to find the propellant consumption to reach a Lunar orbit, starting from GEO with an initial delta-V of about 1.2 km/s; this informs the space-craft design, imposing requirements on propellant storage, Attitude Control Systems, propulsion performances and others. Finally, the mission architecture, which includes the LPS constellation, general system design and a mission cost analysis are presented.

2 Propulsion System

2.1 Electron-Cyclotron Resonance Thruster

The ECRA is an electrode-less electric propulsion device that was first investigated for possible spacecraft propulsion in the 1960s [4, 5]. Unfortunately, the main obstacle to its development was the massive and inefficient microwave power generators in comparison with other direct current power supplies, which undoubtedly prompted the rise of other electric propulsion devices, such as ion or hall thrusters. Besides this fact, the ECRA presents very positive characteristics, as the highly efficient wave-plasma coupling [4] or the absence of a neutralizer. This has encouraged different research efforts to focus again on ECRA technology during the past years [6, 7, 8].

Currently, significant work regarding the technology of the ECRA is being carried out in order to increase its Technology Readiness Level (TRL). First, the development of solid state amplifiers allows for compact power supplies, since there is no need for the traditional vacuum tubes. These developments make the idea of providing microwave power inside a 1U CubeSat feasible. Furthermore, important research on magnetic nozzles has been done during the past ten years [9], highlighting their capabilities as highly efficient, current-free, acceleration mechanisms.

The ECRA under development by ONERA has the particularity of a coaxial geometry design, reducing its size in comparison with other wave-guide ECRA [10], and enabling its operation in the low power consumption (ranging 10-30 W). Furthermore, it has showed greatly encouraging performances, already comparable to other electric thrusters in similar power ranges.

The main motivation of using an ECRA to propel a Cubesat is its compact design, which excludes grids, electrodes and neutralizers, and relies very few (moving) components (mainly related to the propellant storage and injection sub-systems). This allows to easily scale it down and significantly reduces the required volume for the propulsion module.

2.1.1 ECRA Design

Electrons in a magnetic field perform a gyromotion with a characteristic frequency $\Omega_e = eB/m_e$. Tuning a micro-wave source to this frequency creates a resonance, efficiently coupling energy to the electrons. For a

common 2.45 GHz power source, this can be achieved with a magnetic field of 875 G.

In the current ECRA design, the magnetic field B is provided by a Neodymium permanent magnet, which creates the resonance zone, but also the magnetic nozzle responsible for ion acceleration. The microwave power is transmitted to the plasma by a coaxial transmission line. The design proposed in this paper is based on the current design being tested at ONERA. A coaxial cable ends in a conical cavity with an external connector of 27 mm diameter and an internal connector of 3 mm diameter. The length of the source is 15 mm. For illustration, a simple CAD design and a schematic of the thruster are shown in Figures 1(a) and 1(b).

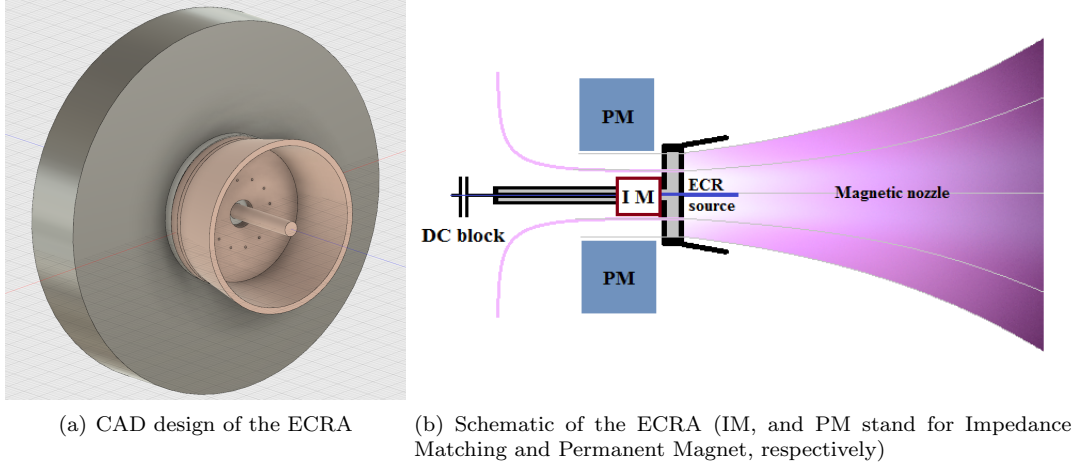


Figure 1: ECRA CAD design and schematic.

2.2 Subsystem Design and Enabling Technologies

2.2.1 Micro-Wave Generator

The nominal operating power for the thruster is around 30 W for current efficiency levels. The possibility of throttling the thruster, for station keeping purposes, for example, should also be considered. The power unit consists of a solid state microwave amplifier, together with a 2.45 GHz oscillator, a tuner and a cooling system. Nowadays, microwave solid state amplifiers are commercially available; however the efficiencies do not presently exceed 40% [11]. It is expected that amplifiers with a efficiency exceeding 80% or possibly higher will be available in the near future as it is an expanding field of research.

2.2.2 Transmission Line

A 50Ω coaxial line connects the plasma source cavity with the microwave power source output. To isolate the power supply and its components from the plasma source, a Direct Current Blocker (DC Block) is used. This allows the thruster to be electrically floating, with potentials around 100-200 V. To prevent conduction heating in the permanent magnet, the authors propose a ceramic junction between the magnet and the outer connector (See Fig 1(b)). An impedance matching system between the 50Ω coaxial line and the plasma source, was also added to the original ONERA design to maximize the total power transmitted to the plasma at different operating conditions.

2.2.3 Propellant

One of the main advantages of the ECRA is the fact that it is a cathode-less device; this allows for an extended lifetime even when using low purity propellants, as this is typically a problem of hollow cathode neutralizers, due to potential poisoning of electron emitting materials. The existing thruster components are not susceptible to damage from most propellants, which opens the range for new possibilities and reduces the constraints on the purity grades used.

In terms of performance, there are two main points to take into account when selecting the propellant: The ionization energy and the ion to electron mass ratio. The first one is important to achieve high ionization efficiencies. The second one is related with the kinetic ion energy throughout the magnetic nozzle, which is not initially evident unless looking into the physics of Magnetic Nozzles. As it is currently understood, the main ion acceleration mechanism in the magnetic nozzle is due to the ambipolar electric potential that is developed throughout the expansion [12, 13]. Navarro et. al [14] demonstrated that this potential drop was almost linear with the logarithm of the ion to electron mass ratio, and so with the final ion kinetic energy under the collisionless regime. Jarrige et. al. [15] have tested the ECRA with Argon and Xenon, obtaining higher performance with Xenon. A widely proposed alternative for compact propulsion systems is to use Iodine, which is cheaper than Xenon or Argon, has a similar atomic mass to Xenon, a lower ionization energy than either, and may be stored in solid state; Grondein [16] reported some benefits to the use of this propellant in terms of thruster performance for the PEGASES engine. Furthermore, using iodine would also allow the presence of a high pressure vessel in the CubeSat.

A comparison table between the three elements is provided for reference:

Propellant	Atomic Mass (u)	First Ionization Energy (eV)
Xenon	131	12.12
Argon	40	15.75
Iodine	126	10.45

Table 1: Characteristics for several propellant candidates

2.3 Propulsive Performance

The highest thruster efficiency achieved up to now with the ECRA of ONERA is around 17%, with a total specific impulse of $I_{sp} = 1000$ s, and a thrust to power ratio of 32.8 mN/kW [17]. The maximum thrust estimated is around 1 mN. Table 2 compares this performance with similar electric thrusters that are being already commercialized. The thruster efficiency has been calculated according to the following formula [18]:

$$\eta_T = \frac{T^2}{2\dot{m}_p P_{in}} \quad (1)$$

where T stands for thrust, \dot{m}_p for propellant mass flow and P_{in} for total injected power; the thrust efficiency does not take into account the efficiency of the power supply system. As may be seen in Table 2, the ECRA from ONERA compares well in performance despite the early stage of development. It should be noted that lifetime of ECRA as not been investigated yet.

Indeed, the current version of ECRA delivers a high throughput at reasonably high efficiency, for the lower end of the Isp range. It is worth noting in Table 2 that the Tile 5000 AS is an Electrospray type thruster.

To extrapolate the effect on the ECRA performances when implementing the ideas addressed in this article, it is necessary to break down the thruster efficiency in different parts. The experimental data for the actual ECRA can be found in [17]. Since the development of these technologies is in its infancy, it can be challenging to perform a technical extrapolation; it is possible, however, to roughly estimate future performance gains by identifying the main efficiency losses and how they may be improved.

Thruster	I_{sp} (s)	TTPR (mN/kW)	P (W)	T (mN)	\dot{m}_p (mg/s)	η_T (%)
ECRA ONERA	1000	32.8	30	1.0	0.1	16.6
BIT-1 BUSEK	2150	10	10	0.1	0.005	10.2
IFM 350 Nano	3000	10.6	32	0.34	0.01	16.4
Phase 4 RFT	520	12.5	40	0.5	0.1	3.13
Tile 5000 AS	1500	60	25	1.5	0.1	45

Table 2: Performance of several existing electric thrusters compared to ECRA from available online datasheets

- **Mass efficiency η_M :** It is defined as the ratio between ion and injected gas mass flows. It expresses the thruster capability to ionize and produce ion thrust. Currently, the mass efficiency of the ECRA is 62%. The authors argue that an optimization of the source geometry and materials, as well a correct combination of nominal power and mass flow could possibly result in $\eta_M \sim 90\%$, without penalizing ion energy or thrust.
- **Divergence efficiency η_D :** It takes into account the fact that the beam is not perfectly collimated. It is defined as the ratio between the total beam power and the fictitious power if the plume was completely collimated in the axial direction. The ECRA divergence efficiency is currently 83%. Optimizing the magnetic topology to decrease the divergence can improve this figure. New 3D printed magnet technology could be valuable in obtaining more complex magnetic configurations. The ideal topology would ensure a constant magnetic field strength in the source region followed by a low to medium divergent nozzle.
- **Energy efficiency η_E :** It relates the total input power to the thruster with the power deposited in the jet. The energy efficiency is currently 38%, however, it is the most complex value to extrapolate, since multiple effects are involved. Since many geometrical parameters (wall surface and shape, materials, etc) are still to be investigated, it is not unreasonable to think that ECRA could reach an energy efficiency around $\sim 50\%$.

Therefore, according to Equation 2, the total thruster efficiency can be expected to increase through further development, reaching a value of $\sim 30\%$ instead of the current 17%.

$$\eta_T = \eta_M \eta_E \eta_D^2 \quad (2)$$

A $\sim 30\%$ efficiency would have tremendous implications for the CubeSat, since it would reduce the power needed for the ECRA, potentially reducing it by almost a half.

2.4 Other Enabling Technologies

2.4.1 Thruster materials

The selection of materials for the outer and inner connectors of the thruster (i.e., the thruster walls) is an important decision, since the electromagnetic waves responsible for heating the electrons by electron cyclotron resonance propagate through this cavity. These materials will be exposed to high plasma temperatures (which peak at about 50 eV in current experiments), so erosion and sputtering must be taken into account. The authors propose, as an enabling technology for long duration missions, to employ new material techniques which might allow for increased sputter protection while maintaining other desirable properties; particularly, electric conductivity, since the metallic walls double as outer conductor of the microwave transmission line. A recent approach towards achieving this goal was reported by Herbig and Michely [19], where they demonstrated sputtering protection through the addition of a Graphene layer over a sheet of Iridium. Though the Secondary Electron Emission properties of such layers would be of importance for the final

selection as a thruster material (due to its distinct effect over plasma properties), the results shown here can be regarded as positive in regards to the use of shielding layers and, in general, Metal Matrix Composites.

2.4.2 Propellant storage

CubeSat dedicated propulsion systems are likely to rely mostly on Iodine as a propellant [20]. For a CubeSat ECRA, aside from the inherent benefits of this propellant as seen from the plasma source and nozzle acceleration mechanisms, the use of Iodine reduces the volume associated to pressurized propellant storage and complexities due to high pressures; in the case of CubeSats these become actual limitations due to restrictions on pressurized gases. Construction and testing of an Iodine feed system for the iSAT 12U CubeSat was reported by Polzin and Peeples [21], where reservoir heating was used together with a flow control valve to achieve control over the Iodine gas mass-flow. Some challenges remain, however, regarding Iodine deposition (solidification) in plumbing and fluid control systems, thermal control and inertia, responsiveness in microgravity conditions, as well as issues due to the highly corrosive nature of the propellant.

3 Trajectory Design

In this section, a procedure to design minimum-fuel Earth-Moon Cubesat trajectories for the mission proposed will be presented. This work follows the systematic approach given in [22] to build low-energy transfers from the Earth to the Moon relying on the theory of the invariant manifolds of the Lagrange points of both the Sun-Earth and the Earth-Moon systems. These trajectories will serve as initial guesses for the subsequent optimization, as in [23], obtaining solutions that are suitable for the micro-propulsion scenario.

3.1 Initial Guess Construction

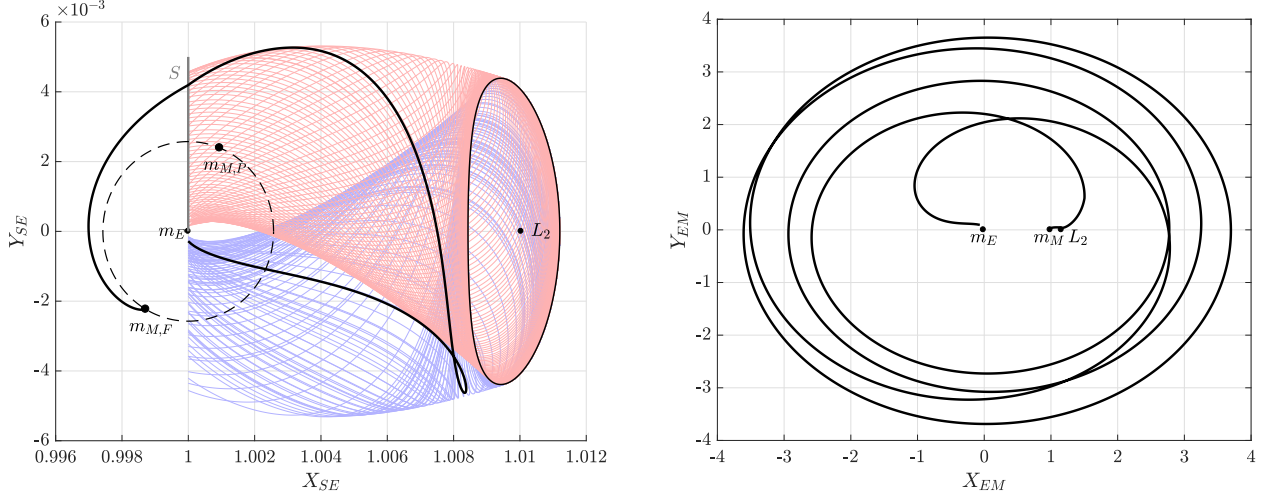
In this approach, the four body problem is split into two Planar Circular Restricted Three-Body Problems (PCR3BP) and therefore the transfer trajectory is naturally divided into two sections: the Earth escape leg, described in the Sun-Earth PCR3BP, and the Moon capture leg, described in the Earth-Moon PCR3BP. At a later stage, the trajectories constructed in the two different systems are patched by examining the intersection of the manifolds phase space in a given section. The *planar* and *circular* characteristics of the model do not affect significantly the applicability to the problem at hand, since the eccentricities of the Earth and Moon orbits are just 0.0167 and 0.0549, while the Moon orbit inclination is only 5° from the ecliptic.

The transfer starts at GEO, where the launcher upper stage provides a ΔV_0 that inserts the spacecraft into a trajectory towards the Moon. In order for that trajectory to be *almost* ballistic, the concept of *orbit twisting* is used [22]. The obtained initial guess for this case is depicted in Figure 2 and corresponds to a transfer of 155 days. As it can be seen, the Cubesat escapes the Earth following the Sun-Earth L_2 internal stable manifold, twists and then follows the Sun-Earth L_2 internal unstable manifold up to the patching section S , where it connects with the Moon capture leg that approaches the Moon following the Earth-Moon L_2 stable external manifold.

3.2 Optimization

The goal of the optimization process is to obtain the thrust magnitude and direction that will allow the spacecraft to perform the Earth-Moon transfer with the lowest fuel consumption consistently with the Planar Bicircular Restricted Four Body Problem (PBRFBP) dynamics and the appropriate constraints. For that, a direct transcription or collocation method, particularly the Hermite-Simpson approach, was used in conjunction with the solver IPOPT (Interior Point Optimizer).

The dynamics of the optimization problem are the ones in eq. (3), where $m_s = 3.28900541 \cdot 10^5$ is the scaled mass of the Sun, $\rho = 3.88811143 \cdot 10^2$ is the scaled Sun-(Earth+Moon) distance, $\omega_s = -9.25195985 \cdot 10^{-1}$



(a) Trajectory in the Sun-Earth synodic system. $m_{M,F}$ and $m_{M,P}$ refer to the Moon position at the end of the trajectory and at the patching instant; (—) Moon's orbit; Sun-Earth L_2 interior stable (—) and unstable (—) manifolds; (—) Patching section S ; L_2 represents the Sun-Earth L_2 libration point.

(b) Trajectory in the Earth-Moon synodic system. m_E and m_M refer to the Earth and Moon masses, L_2 represents the Earth-Moon L_2 libration point.

Figure 2: Complete trajectory starting from a GEO orbit, selected Initial Guess for trajectory optimization.

is the scaled angular velocity of the Sun and $\mu = 1.21506683 \cdot 10^{-2}$ is the Earth-Moon mass parameter [24]. Characteristic magnitudes are $DU = 3.844 \cdot 10^8$ m, which is the Earth-Moon distance; $TU = \frac{T}{2\pi} = 4.348$ days, where T corresponds to the Earth-Moon orbital period; and $MU = 6.0458 \cdot 10^{24}$ kg, which corresponds to the Earth-Moon total mass.

$$\begin{aligned} \ddot{x} &= \frac{\partial \Omega_4}{\partial x} + 2\dot{y} + \frac{\pi T_{max} \cos \theta}{m}, & \ddot{y} &= \frac{\partial \Omega_4}{\partial y} - 2\dot{x} + \frac{\pi T_{max} \sin \theta}{m}, & \dot{m} &= -\frac{\pi T_{max}}{I_{sp} g_0} \\ \Omega_4(x, y, t) &= \Omega_3(x, y) + \frac{m_s}{r_3(t)} - \frac{m_s}{\rho^2} (x \cos(\omega_s t) + y \sin(\omega_s t)) \\ \Omega_3(x, y) &= \frac{1}{2}(x^2 + y^2) + \frac{1-\mu}{r_1} + \frac{\mu}{r_2} + \frac{1}{2}\mu(1-\mu), & r_3 &= [(x - \rho \cos(\omega_s t))^2 + (y - \rho \sin(\omega_s t))^2]^{1/2} \end{aligned} \quad (3)$$

In these equations, T_{max} and I_{sp} are the maximum thrust and the specific impulse of the spacecraft propulsion system, and g_0 is the standard acceleration due to gravity on the surface of the Earth. Then, the controls of the system are the following: π , which is the throttle of the propulsion system, and θ , which is the angle made by the thrust vector with the Earth-Moon synodic reference frame x-axis.

The dimensions of this optimal control problem are the following: $\mathbf{x}(t) \in \mathbb{R}^5$, $\mathbf{u}(t) \in \mathbb{R}^2$, $\mathbf{p} \in \emptyset$. In other words, the state is a vector of five components, namely, x and y position and velocity, and spacecraft mass; and the control vector is composed by the thrust throttle ($0 \leq \pi(t) \leq 1$) and the thrust direction angle ($0 \leq \theta(t) \leq 2\pi$).

In this case, the goal was to minimize the fuel consumption, since the amount of fuel needed to carry onboard is a very important factor concerning the overall cubesat size and weight limitations. Therefore, the objective function to be minimized was the following:

$$J = -m_f \quad (4)$$

3.3 Results

In order to arrive at our target orbit, which corresponds to a circular lunar orbit of 4000 km radius, the optimization problem described above is subjected to a set of boundary conditions. In this way, we constrained the initial position to be placed at GEO altitude (eq. (5)) and the initial external burn to be parallel to the velocity at that GEO orbit (eq. (6)). Finally, the magnitude of the initial impulse is bounded to a reasonable value (eq. (7)). Note that a small tolerance $\epsilon = 10^{-20}$ has been used with some constraints in order to avoid convergence issues coming from the fact that there is a finite numerical accuracy associated with the computations.

$$r_{GEO} - \epsilon \leq \sqrt{(x_0 + \mu)^2 + y_0^2} \leq r_{GEO} + \epsilon \quad (5)$$

$$| (x_0 + \mu)(\dot{x}_0 - y_0) + y_0(\dot{y}_0 + x_0 + \mu) | \leq \epsilon \quad (6)$$

$$\begin{aligned} 0 \leq \sqrt{(\dot{x}_0 - y_0 + V_{GEO} \sin \gamma_0)^2 + (\dot{y}_0 + x_0 + \mu - V_{GEO} \cos \gamma_0)^2} &\leq \frac{1}{2} V_{GEO} \\ V_{GEO} &= \sqrt{\frac{1 - \mu}{r_{GEO}}}, \quad \gamma_0 = \tan^{-1}(y_0, x_0 + \mu) \end{aligned} \quad (7)$$

Concerning the final state, eq. (8) and eq. (9) were imposed in order to limit the final orbit radius to our target (adding some tolerance for convergence issues), and to make sure the final velocity is consistent with the lunar orbit we are aiming at.

$$3950 \cdot 10^3 / DU \leq \sqrt{(x_f - 1 + \mu)^2 + y_f^2} \leq 4050 \cdot 10^3 / DU \quad (8)$$

$$\sqrt{((\dot{x}_f - y_f) + V_c \sin \gamma)^2 + ((\dot{y}_f + x_f + \mu - 1) - V_c \cos \gamma)^2} \leq \epsilon \quad (9)$$

where R_{moon} is the radius of the Moon, and $V_c = \sqrt{\frac{\mu}{r_f}}$.

Figure 3 depicts the results obtained from the optimization when using characteristic values for the ECRA thruster ($I_{sp} = 1000$ s and $T_{max} = 1$ mN) and two values for the initial mass of the Cubesat, 3 kg and 6.5 kg, which represent some sort of reference for the minimum and maximum initial weights for a 3 U Cubesat. Note that ψ represents the angle between the thrusting direction and the instantaneous velocity direction; this imposes a requirement on the Attitude Control System (ACS): as the thruster design does not include vectoring capabilities control is achieved through angling of the space-craft's own axis. At the same time, Table 3 gathers some characteristic magnitudes for those two examples presented.

m_0	ΔV_0	Transfer time	m_f/m_0
3 kg	1.1772 km/s	155.7 days	0.9590
6.5 kg	1.1436 km/s	156 days	0.8668

Table 3: Details of optimized trajectories.

As it can be seen, the initial impulse and transfer time are very similar for both m_0 values. Indeed, the greatest difference between the two solutions lies on the propellant mass consumption (Figure 3(b)). Indeed, the 6.5 kg Cubesat arrives at lunar orbit with just 86.7% of its initial mass. This is of course highly tied to the throttle evolution observed in Figure 3(c), where there is a notable difference between the two solutions. For the 3 kg Cubesat, the thrust needed is less than 30% the maximum one up to the final 20 days of transfer, where periods of maximum throttle are observed. On the contrary, the throttle evolution for the 6.5 kg Cubesat trajectory is quite smooth and it results in a less efficient transfer. A plausible explanation for this behaviour could be that the Cubesat mass is too large for the orbital corrections to concentrate on the final stages of the trajectory (note that for the case of 3 kg, $\pi = 1$ is needed at some points) and

therefore those corrections are provided in a more uniform way during the transfer. In other words, the 3 kg Cubesat is small enough with respect to the ECRA thrusting capacity so that the optimized low-thrust transfer resembles more a geometrically similar two-burn impulsive trajectory.

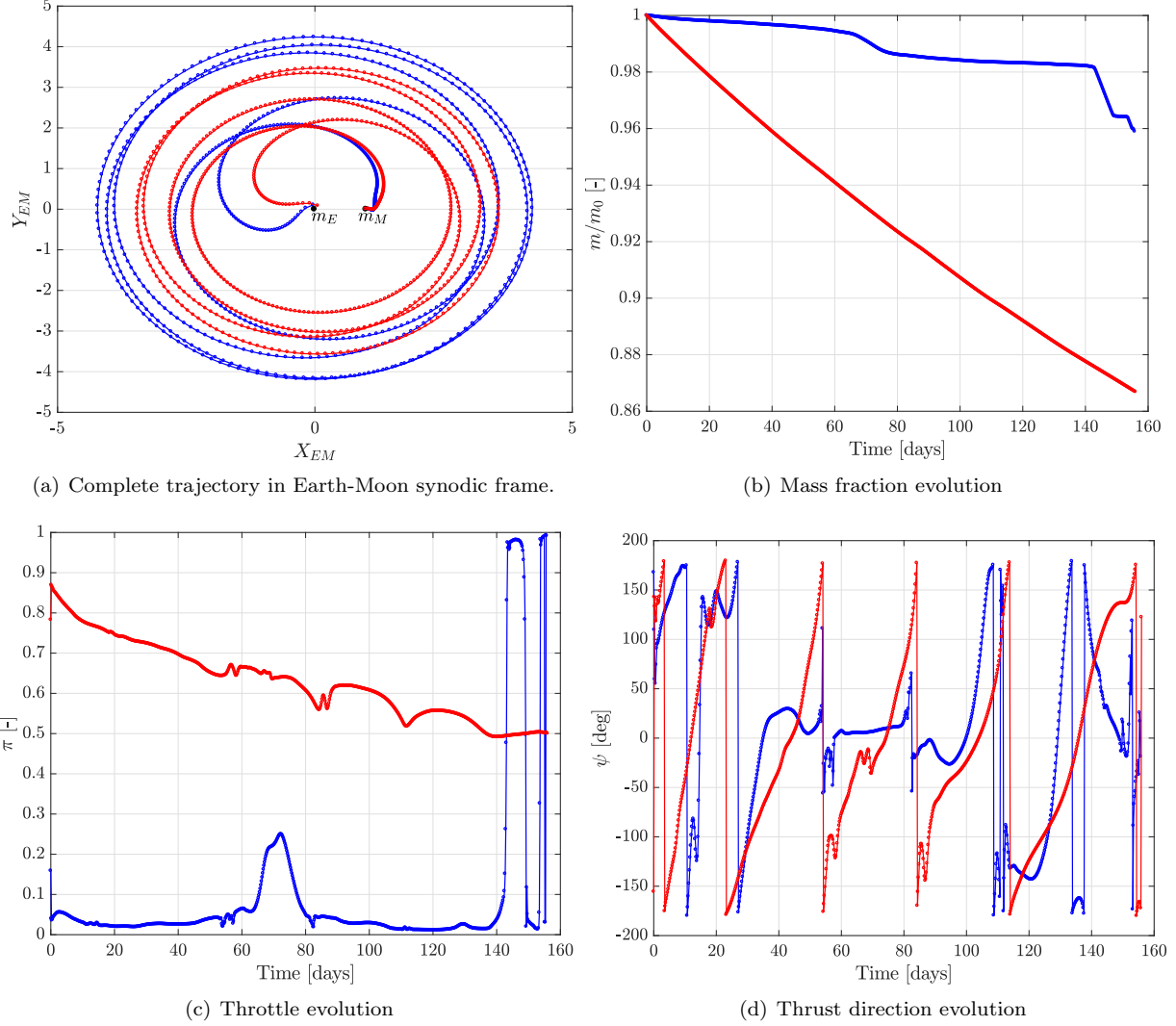


Figure 3: Optimization results for a (—) 3 kg Cubesat and a (—) 6.5 kg Cubesat.

The analysis presented here can be further optimized in a concurrent manner together with the CubeSat design: throttling capacities of the thruster and limitations on the ACS could be included, considering, for example, no throttling (thruster ON or OFF only) and CubeSat orienting restricted to ± 20 deg. This bridge between the trajectory design and the CubeSat's capabilities is fundamental to arrive at a final design which stands at the intersection between the mission's requirements and the hardware's capabilities.

4 Mission Architecture

4.1 Constellation Design

The current LPS constellation partially emulates the GPS design. To allow future users to rely on Commercial off-The-Shelf (CoTS) receivers, the same frequency and signal protocols as for GPS (and Gallileo) are used. The LPS constellation will have a minimum of 4 satellites visible from any position on the Lunar sphere and at any given time. Furthermore the appropriate signal (L1,L2) broadcast from the satellites should reach the Lunar surface with a signal strength above -160 dBW (GPS receiver limit).

There are many different constellations possible for providing full coverage of a celestial body. The most popular is the Walker-Delta or Rosette constellation which consists of p number of equally spaced orbital planes all with inclination i , each plane having n number of satellites, for a total of $N = np$ satellites. Satellites in subsequent planes have a phase difference $\frac{2\pi}{N}m$. Here $0 < m < N - 1$ is an integer. The notation according to Ballard is $i : N/p/m$ [25]. Such constellations are not the only possible solution for an LPS. Romagnoli and Circi proposed a constellation of 8 satellites in Lissajous orbits around the Lunar L1 and L2 Lagrange points. [26] However L1 and L2 are more than 60.000 km away from the moon and the satellites would require high power and/or directional antennas.

To achieve the LPS constellation with Cubesats the required antenna should be low power (10 W) and near-isotropic to avoid continuous pointing which would put a strain on the ADCS. An additional benefit of a near-isotropic antenna is that the signal also penetrates into space making it available to Lunar-bound spacecraft.

Free-space path loss of an isotropic signal is given by:

$$FSPL(dB) = 20 \log_{10}(d) + 20 \log_{10}(f) + 20 \log_{10}\left(\frac{4\pi}{c}\right) \quad (10)$$

A 10W antenna equals 10dBW and to achieve a signal of more than -160dBW the FSPL has to be less than -165dB (where a 5 dB margin was imposed). For the L1 signal (1575.42 MHz) the maximum distance is: 2692 km resulting in a maximum orbital radius of 4429 km. The GPS system has an orbital radius of 26.600 km which has an orbital period of 12h or half a synodic day ensuring that the satellites passes over the same point twice a day. Due to tidal locking the lunar day is 27.3 days and tuning the constellation to this period is impossible.

The main drivers for the orbital radius are therefore the signal strength and the visibility. For simplicity an orbital radius of 4000 km was chosen, well within maximum of 4429 km. Obviously this parameter can be optimized for together with the available antenna power. Including continuous nadir pointing puts some strain on the ACDS but allows for a directional antenna, a larger orbital radius and increased visibility (or reduced number of satellites). The optimal configuration needs to be optimized for, concurrently with the satellite system design.

A 60° : $24/4/1$ constellation at an orbital radius of 4000 km is shown in figure 4(a). Taking into account a minimum elevation of 10° it would provide a continuous visibility of at least 5 satellites at the Lunar poles as can be seen in figure 4(b).

4.1.1 Station Keeping Requirements

Due to perturbing forces some station keeping might be necessary to maintain the constellation. To analyze this the satellites' positions were calculated using a Cowell-propagator taking into account the Lunar spherical harmonics, solar-radiation pressure and third-body perturbations from the Sun and the Earth. It was found that the orbital radius was remarkably stable within ± 1 km, that the RAAN progression was similar for all 4 planes, and that the orbit remained (near-)spherical ($\epsilon < 3 \cdot 10^{-3}$). The main perturbation is on the inclination which can change up to 2° per year.

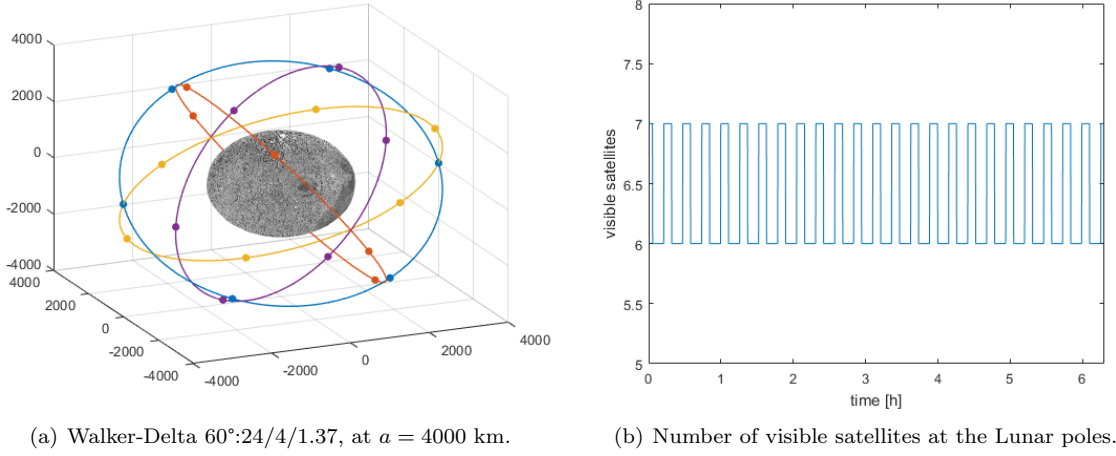


Figure 4: Simulation of a Walker-Delta constellation at 4000 km and satellites visibility at the Lunar poles.

With a dry mass of 4.5kg (see section 4.2) and a mass limit of 6.5kg the satellites are left with 2kg of propellant. From table 3 it clear that the propellant consumption for the orbit insertion is 13% of the initial mass such that the Cubesat is left with 1.134 kg of propellant.

The delta-V for a plane change at low thrust is given by [27]:

$$\Delta V = V_0 \sqrt{2 - 2 \cos \frac{\pi}{2} i} \quad (11)$$

Which for an inclination of 60° results into $1.47V_0$ where V_0 is the orbital velocity of 1.107 km/s, so the $\Delta V = 1.62$ km/s. From Tsiolkovsky's equation we find that this requires 1.01 kg of fuel. Leaving the satellite with 124g of fuel. The delta-v for a yearly 2° inclination correction is 61 m/s. This consumes about 28g per year and therefore results in a lifetime of about 4-5 years. However performing more frequent orbit corrections could potentially lower the fuel consumption but at the cost of increased satellite down-time.

4.1.2 Ground Segment

The GPS has an extensive ground segment including two control centres, 6 monitoring stations and 4 antennas. Such thorough control of the GPS constellation is warranted due to its high cost (\$12 billion), military importance and its enormous impact on the world economy. However the LPS system could be operated with a significantly smaller ground segment. Nonetheless, to ensure accurate position information the satellite positions need to be tracked and updated. One of the enabling technologies for a Cubesat based positioning system are chip-scale atomic clocks (CSACs). These low power miniaturized clocks easily fit in a Cubesat and their accuracy is rapidly approaching that of the larger clocks. However these CSACs need to be synchronized regularly to correct for clock drifts.

The cheapest solution would be to track the satellites from Earth. However, accurate tracking from Earth of Cubesats in Lunar orbit using passive radar ranging seems implausible if not impossible; Laser ranging might be an option, requiring the satellites to be outfitted with retro-reflectors. Active tracking would require both more power and active pointing on the side of the satellite which is probably only feasible with a 6U CubeSat. The more obvious but expensive option would be to build a tracking station on the Lunar surface, but this would (partially) negate the low-cost Cubesat concept. One larger spacecraft in the L1 point as a space-based tracking station might provide a middle way.

4.2 Mass Budget

The trajectory optimization was done for a 3 kg and a 6.5 kg space-craft; the actual CubeSat standard is 1.33 kg per 1U, meaning a total of 4 kg for a 3U configuration. However, the possibility of waiving some of these standards exists, hence the high upper-mass used in our calculations. Nevertheless, we include an initial mass budget for each of the CubeSats in the constellation, based on the required on-board systems; we include an approximate cost for reference, based on Commercial Off The Shelf (COTS) components sourced from cubesatshop.com:

Item	Mass (g)	Aprox. Cost (k\$)
Structure	300	4
Deployable Solar Panels	1600	60
Batteries	150	5
On-Board Computer	100	10
Monopole Antenna	100	5
Transmission System	75	10
Power Processing Unit	80	5
Star-tracker(x2)	50	3
Atomic Clock	50	3
Attitude Control System (Inertial wheels + Cold Gas)	500	100
ECRA Thruster	900	?
Radiator	200	?
Propellant storage, mass-flow controller, plumbing	200	?
Microwave generator, transmission line	200	?
<i>Total</i>	~ 4500	> 205

Table 4: LPS CubeSat mass & hardware cost budget

Some further comments can be made regarding this mass/cost budget: In general, the cost of the propulsion subsystem (Engine, Propellant storage, mass-flow controller, plumbing and Radiator) is difficult to estimate at this stage since development and qualification costs would be factored into the "consumer price". The use of a radiator or heat-rejection mechanism is based on our current experience with the ECRA model thruster and the temperatures reached during operation. The sizing of the radiator is beyond the scope of this paper and its mass is considered a conservative estimate; a final design might benefit from high-efficiency and high-temperature heat dissipators, based on new materials such as carbon fibres, as being developed by NASA. A Microwave generator "on a chip", the TDE001 by ISM, was identified as a suitable candidate for the requirements of ECRA thruster, pricing and "space grading" were not found, however; the space grade issue is also applicable to the Atomic Clock.

The final mass budget is on the limit of the desired "dry" mass, if we are to take into account the Moon transfer, orbital plane changes and the requirements for Station Keeping (Section 4.1.1). Together with the limitation imposed on the power budget due to current efficiency levels demonstrated for the thruster, it is possible that the system design would benefit from a 6U architecture in order to release some of the constraints on the system; we leave this decision for a future iteration of the constellation design.

4.3 Cost Analysis

Constellation mission architectures using Cubesats are yet to be materialized by commercial companies and space agencies alike. Presently, nanosatellites are launched "piggy-backing" off of larger launches (with a number of available platforms), or ejected from the ISS using the NanoRacks CubeSat Deployer at *Kibo* module; some of these launches are deemed educational and covered (fully or partially) by programs such as NASA's Educational Launch of Nanosatellites (ELaNA) or ESA's Fly Your Satellite! (FYS). In addition, hardware cost depends heavily on the type of satellite being built (educational vs. non-educational) and on whether the CubeSat's systems are sourced mainly from COTS or custom built. This also relates to the

post-launch mission control, mission lifetime and, in our case, additional considerations required for the LPS constellation (e.g., "Ground control").

In summary, since the suspected paradigm shift due to miniaturization is still ongoing, including the development of dedicated launch platforms, hardware standards and others, the final mission cost is still highly speculative.

4.3.1 Launch Cost

Starting with launch costs, a 2016 report by the Satellite Industry Association [28] cites capabilities for some of the most serious contenders for the $< 500\text{kg}$ -to-LEO segment of the market (note that not all of these launch vehicles include a second stage):

Platform (Provider)	Capacity to LEO (kg)	Price ($\text{k\$}/\text{kg}$)
PegasusXL (Orbital ATK)	440	30
LauncherOne (Virgin Galactic)	400	25
Alpha (Firefly Space Sys.)	400	20
Electron (Rocket Lab)	150	32
Bloostar (Zero2Infinity)	150	26
Haas 2C (Arca Space Corp.)	100	10

Table 5: Very Small Launch Vehicles

Launch platforms relevant to this project offer payload mass to LEO ranging $100\text{kg} - 400\text{kg}$ at prices ranging $\$10\text{k}/\text{kg} - \$40\text{k}/\text{kg}$; i.e., the average price-per-kg is not necessarily reduced from traditional launchers. Nonetheless, these platforms may offer a cost improvement over the piggy-back option (which according to [spaceflight.com](#) [29] averages at ~ 300 k\\$ to LEO and $\sim \$900$ k to GEO for a 3U Cubesat) and, of course, offer the advantage of a dedicated solution, both technically and logically, which may be tailored to the requirements of a bold mission statement such as the LPS.

Our flight plan requires of an initial impulse at GEO of ~ 1.2 km/s, which in the case of the 6.5Kg, accounts for about half to the total ΔV budget for the GEO-to-Lunar-orbit transfer; this initial impulse could be achieved through a third stage. If we assume an average payload mass at GEO that is 40% that of the LEO capability, given in Table 5, which is a typical value for the GEO/LEO payload mass-ratio in traditional launchers, then, assuming the 400 kg LEO capacity and the use of a third stage consisting of, conceptually, a CubeSat dispenser and a typical apogee engine with $I_{sp} = 300$ s, weighting 20% of the initial third stage mass, using Tsiolkovsky, we may obtain a total weight injected into Lunar transfer orbit of:

$$\Delta V = I_{sp} g_0 \ln \frac{m_0}{m_f} \rightarrow m_{constellation} = 0.8 \frac{0.4 \cdot 400\text{kg}}{\exp \left(\frac{1200\text{m/s}}{300\text{s} \cdot 9.8\text{m/s}^2} \right)} \approx 76\text{kg} \quad (12)$$

Since the total maximum estimated constellation mass for 24 satellites is ~ 156 kg, two to three launches of the larger capacity vehicles shown in Table 5 would suffice for launching the LPS constellation. The *very* speculative price tag for this part of the operation is on the order of \$16m-24m for the most affordable option, not taking into account insurances and other factors. Again, this cost is comparable to the piggy-backing option to GEO, with the exception of the initial injection, for which a dedicated launcher will be surely required, either to carry the third stage and constellation or to use the actual second stage for the initial injection as an alternative; in both cases, this represents a show-stopper for the piggy-back option and a requirement on the launch platform, since a second stage and GEO capability are a necessity. The estimate for the dedicated third stage cost, if used, remains outside of the scope of this paper.

4.3.2 Constellation Cost

A number of cost-estimate methodologies for CubeSats have been developed in recent years: AMES Cost Model (NASA Ames), COMPACT (Jet Propulsion Laboratory), A-PICOMO and SSCM (The Aerospace Corporation) etc. These are based on statistical analysis performed on cost of readily deployed satellites procured by a number of institutions and additional mission costs post launch.

An analysis using SSCM [30] is expected to be completed in the future, adding cost estimates on the constellation qualification round and post-launch costs. For the purpose of this paper, however, we may estimate each satellite to be on the order of $\sim \$400k$, based on the hardware cost budget in Table 4; the total constellation cost is therefore in the order of \$10m. The mission price tag will, of course, increase if we take into account the requirement of a “ground station”, either at the Moon or in the L1 point, as was mentioned in Section 4.1; the estimation of the cost for this segment is outside of the scope of this paper.

5 Conclusions

This paper explores the possibility of performing Lunar Cubesat missions with electric propulsion thrusters, in order to envision the strong advantages of electric propulsion versus CoTS chemical systems, which are limited either due to low I_{sp} or by regulations. To provide insight on this idea, a technical analysis regarding the development of a Lunar Positioning System with a 24 CubeSats constellation has been carried out.

The thruster selected for this mission is the Electron Cyclotron Resonance - Magnetic Nozzle Accelerator, since it is an emergent technology which, despite its level of development, presents interesting characteristics to be considered as a CubeSat propulsion candidate, such as no moving parts, very few components, simple design or no need for a neutralizer; furthermore, recent research on microchips RF amplifiers makes feasible the idea of providing low power microwave inside a 1U CubeSat. Continued development of the technology may position it as a serious contender even against electrospray systems, which currently hold great promise for this type of mission scenarios. An initial and thorough “white paper” analysis, including thruster design and performance, PPU, propellant storage and materials is carried out in this paper, providing an insight of its future capabilities according to the development of enabling technologies.

This manuscript also contains a detailed Earth-Moon transfer solution optimizing fuel consumption consistently with the Planar Bicircular Restricted Four Body Problem. Taking into consideration the best performance of the ECR Thruster demonstrated until now ($I_{sp} = 1000$ s and $T_{max} = 1$ mN), an optimized solution has been achieved for two different initial masses: 3 kg and 6.5 kg satellites, obtaining a similar total transfer time of 156 days with an initial impulse around 1.15 km/s for both. However, while the 3 kg CubeSat arrives at lunar orbit with 95.9 % of its initial mass, the 6.5 kg CubeSat reaches the same point with only 86.7 %. Regarding the constellation design, a Walker-Delta constellation with 24 CubeSats at 4000 km of orbital radius is chosen, which we have demonstrated to provide a continuous visibility of at least 4 satellites at the Lunar poles.

Finally, a rough cost analysis is carried out, estimating a total constellation cost of \$10m and an additional \$20m for launches using upcoming dedicated platforms.

Further work will be focused on deeper insight into the concurrent mission-trajectory-spacecraft design in order to fully characterize how the performances and limitations of each of the three lead to a constrained solution space that may be optimized. In parallel, further development of the ECRA is ongoing through the MINOTOR H2020 european project and will hopefully see the characterization of the various physical mechanisms though the use of simulation tools and extensive testing; the implementation of the proposed ECRA design and optimization of various efficiencies is also expected.

6 Acknowledgments

The authors would like to acknowledge Dr. Manuel Sanjurjo Rivo for his help and very useful insights into orbital dynamics and space-craft constellations. Additionally, our thanks go to Tania Watson and Alejandro Grande for their help with the video required as part of the Young Visionaries IEPC2017 competition.

References

- [1] E. Kulu, “nanosats.eu,” 2016.
- [2] D. C. Folta, N. Bosanac, A. Cox, and K. C. Howell, “The lunar icecube mission design: construction of feasible transfer trajectories with a constrained departure,” 2016.
- [3] J. Hernando-Ayuso, S. Campagnola, T. Ikenaga, T. Yamaguchi, Y. Ozawa, B. V. Sarli, S. Takahashi, and C. H. Yam, “OMOTENASHI trajectory analysis and design: Landing phase,” in *26th International symposium on Space Flight Dynamics, held together the 31st International Symposium on Space Technology and Science*, no. 2017-d-050, (Matsuyama, Japan), 3-9 June 2017.
- [4] H. Kosmahl, D. Miller, and G. Bethke, “Plasma acceleration with microwaves near cyclotron resonance,” *Journal of Applied Physics*, vol. 38, no. 12, pp. 4576–4582, 1967.
- [5] M. Nagatomo, “Plasma acceleration by high frequency electromagnetic wave in static magnetic field gradient,” in *Space Technology and Science*, p. 57, 1968.
- [6] J. C. Sercel, *An experimental and theoretical study of the ECR plasma engine*. PhD thesis, California Institute of Technology, 1993.
- [7] H. Kuninaka and S. Satori, “Development and demonstration of a cathodeless electron cyclotron resonance ion thruster,” *Journal of Propulsion and Power*, vol. 14, no. 6, pp. 1022–1026, 1998.
- [8] F. Cannat, T. Lafleur, J. Jarrige, P. Chabert, P.-Q. Elias, and D. Packan, “Optimization of a coaxial electron cyclotron resonance plasma thruster with an analytical model,” *Physics of Plasmas*, vol. 22, no. 5, p. 053503, 2015.
- [9] M. Merino Martínez, *Analysis of Magnetic Nozzles For Space Plasma Thrusters= Análisis de Toberas Magnéticas para Motores Espaciales de Plasma*. PhD thesis, Aeronauticos, 2013.
- [10] J. Jarrige, P.-Q. Elias, F. Cannat, and D. Packan, “Characterization of a coaxial ecr plasma thruster,” *AIAA Paper*, vol. 2628, p. 2013, 2013.
- [11] N. products, “products.nuwaves.com/rf-power-amplifiers,” 2017.
- [12] E. Ahedo and M. Merino, “Two-dimensional supersonic plasma acceleration in a magnetic nozzle,” *Physics of Plasmas*, vol. 17, no. 7, p. 073501, 2010.
- [13] A. V. Arefiev and B. N. Breizman, “Ambipolar acceleration of ions in a magnetic nozzle,” *Physics of Plasmas*, vol. 15, no. 4, p. 042109, 2008.
- [14] J. Navarro-Cavallé, S. Correyero, and E. Ahedo, “Collisionless electron cooling on magnetized plasma expansions: advances on modelling,” in *Proceedings of the 34th International Electric Propulsion Conference*, 2015.
- [15] J. Jarrige, P.-Q. Elias, F. Cannat, and D. Packan, “Performance comparison of an ecr plasma thruster using argon and xenon as propellant gas,” in *Proceedings of the 33rd International Electric Propulsion Conference*, pp. 2013–420, 2013.
- [16] P. Grondein, T. Lafleur, P. Chabert, and A. Aanesland, “Evaluation of iodine as an alternative propellant for gridded electric space propulsion systems,” *Bulletin of the American Physical Society*, vol. 60, 2015.

- [17] F. Cannat, *Caractérisation et modélisation d'un propulseur plasma à résonance cyclotronique des électrons*. PhD thesis, Ecole doctorale de l'Ecole Polytechnique, 2015.
- [18] D. M. Goebel and I. Katz, *Fundamentals of electric propulsion: ion and Hall thrusters*, vol. 1. John Wiley & Sons, 2008.
- [19] C. Herbig and T. Michely, "Graphene: the ultimately thin sputtering shield," *2D Materials*, vol. 3, no. 2, p. 025032, 2016.
- [20] H. Kamhawi, T. Haag, G. Benavides, T. Hickman, T. Smith, G. Williams, J. Myers, K. Polzin, J. Dankanich, L. Byrne, *et al.*, "Overview of iodine propellant hall thruster development activities at nasa glenn research center," in *52nd AIAA/SAE/ASEE Joint Propulsion Conference*, p. 4729, 2016.
- [21] K. A. Polzin and S. Peebles, "Iodine hall thruster propellant feed system for a cubesat," 2014.
- [22] J. E. Marsden, M. W. Lo, W. S. Koon, and S. D. Ross, *Dynamical Systems, the Three-Body Problem and Space Mission Design*. 2006.
- [23] G. Mingotti, F. Topputo, and F. Bernelli-Zazzera, "Low-energy, low-thrust transfers to the Moon," *Celestial Mechanics and Dynamical Astronomy*, vol. 105, no. 1, pp. 61–74, 2009.
- [24] K. Yagasaki, "Sun-perturbed Earth-to-Moon transfers with low energy and moderate flight time," *Celestial Mechanics and Dynamical Astronomy*, vol. 90, no. 3, pp. 197–212, 2004.
- [25] A. H. Ballard, "Rosette constellations of earth satellites," *IEEE Transactions on Aerospace and Electronic Systems*, no. 5, pp. 656–673, 1980.
- [26] D. Romagnoli and C. Circi, "Lissajous trajectories for lunar global positioning and communication systems," *Celestial Mechanics and Dynamical Astronomy*, vol. 107, no. 4, pp. 409–425, 2010.
- [27] T. N. Edelbaum, "Propulsion requirements for controllable satellites," *ARS Journal*, vol. 31, no. 8, pp. 1079–1089, 1961.
- [28] The Tauri Group, "State of the satellite industry report," 2016.
- [29] spaceflight.com, "Schedule & pricing," 2016.
- [30] E. Mahr, A. Tu, and A. Gupta, "Development of the small satellite cost model 2014 (sscm14)," in *Aerospace Conference, 2016 IEEE*, pp. 1–13, IEEE, 2016.